A Method for Analysing and Characterizing the Arc Cooling Effect of Different Gases in Strong Axial Flow With SF$_6$ and Air as Examples

Kaiyuan Zhang [ID], Sili Yao [ID], Yi Wu [ID], *Senior Member, IEEE*, and Jiu Dun Yan [ID], *Senior Member, IEEE*

Abstract—A method of quantifying the abilities of different gases to cool an axis-symmetric arc in strong axial flow is established. It is able to quantitatively account for the contributions of different energy exchange processes, such as convection, conduction, radiation and turbulent mixing, towards arc cooling (i.e., increase of arc resistance) during the current zero period of the interruption process. Applying the method to a decaying SF$_6$ arc and an air arc in a converging-diverging nozzle with the arc current ramped down linearly from 1 kA to zero at a rate of 13.5 A/μs, it is shown that the arc cooling effects of turbulence and radial convection, in terms of the reciprocal of their arc cooling characteristic time ($1/\tau_k$), keep increasing in SF$_6$ in the last 2 μs before current zero, but remain effectively unchanged in air. The arc cooling index (ACI) defined at 1 μs before current zero is found to be 2.59/μs for SF$_6$ and 0.96/μs for air. The SF$_6$ arc resistance at current zero is approximately 4 times that of air under the arcing conditions used in this study.

Index Terms—Arc cooling ability, SF$_6$ alternative gases, supersonic nozzle, switching arc, thermal interruption.

I. INTRODUCTION

A. SF$_6$ and its Alternatives

SF$_6$ is an excellent dielectric and arc quenching gas with low boiling temperature and other physical and chemical properties fit for industrial applications [1], [2], [3]. Its first use in electrical industry was seen in the 1950 s with a voltage level up to 132 kV [4] and its widespread use in extra-high voltage and ultra-high voltage ranges started in the late 1970 s and early 1980 s [5]. Meanwhile, from as early as 1973, SF$_6$ as a trace gas in the upper atmosphere was added to the list of gases with potentially adverse environmental effect [6] and started to be

sampled in the stratosphere under Project AIRSTREAM [7]. A good account of the history of SF$_6$ in the atmosphere can be found in [8]. It is the Kyoto Protocol [9] that officially announced the greenhouse effect of SF$_6$ and since then the environmental impact of SF$_6$ has been attracting more and more attention, leading to its restricted use in electrical industry as proposed by the European Commission [10].

The past 10 years have witnessed an avalanche of activities relating to the replacement of SF$_6$ in electrical apparatuses. Most of them focused on the dielectric behaviour of different gases, especially the g^3 gases and their mixtures [11], [12]. The experimentally measured dielectric strength agrees reasonably well with the prediction [13]. On the switching side, it is a different story. While some test results were obtained [14], [15], the challenge is with the understanding and explanation of the differing interruption performances of different gases. It is evident that circuit breaker design has a significant influence on the interruption capability, however the fact that SF$_6$ has been dominating high voltage switching applications is a far cry that it is the material properties that ultimately underpin its dominance. For example, the differences in material properties between SF$_6$ and air are clear, but how their properties lead to the difference in their interruption capability, especially their thermal interruption capability, remains to be answered. This creates a knowledge gap that has to be filled before a theory is established to define the relative superiority of each gas in terms of their thermal interruption potential, or arc cooling ability in a gas blast environment.

B. Characteristics of Gas-Blast Arcs and Role of Turbulence

Arc quenching is a complicated multi-physics process further complicated by the turbulence phenomenon. There is no analytic solution to the arc governing equations. To computationally study the arc cooling process, certain simplifications have to be introduced. For example, in a commercial gas-blast circuit breaker, at least one hollow contact (tulip contact) is used to ensure firm electrical contact with the other contact (normally a solid plug contact). Such a design provides practical benefits to the operation of the circuit breaker, but it also allows the arc column at low current to deform freely in three-dimensional space. To focus on the influences of material properties on the arc quenching process, a simple nozzle structure with a solid

contact to stabilize the arc root would be preferred, such as the arrangement adopted in [16].

The ultimate objective of using the gas blast principle is to cool the arc and increase its electrical resistance rapidly near current zero to withstand the transient recovery voltage from the network. Among the vast number of publications on switching arcs, the work in [16] and [17] examined a large number of gases for current interruption both theoretically and experimentally under well-defined test conditions. The "interruption capability" of these gases, as referred to by the authors, was measured.

Sufficient knowledge of the underlying physical mechanisms involved in switching arcs is essential to meaningful computer simulation. The 1970 s and early 1980 s have witnessed a large volume of optical and spectroscopic diagnosis of switching arcs, focusing on the role of flow turbulence and arc temperature measurement [18], [19], [20], [21]. These studies provided vital information on the dynamic behaviour of switching arcs, especially the dominant role of turbulence in arc cooling [22], [23]. It was categorically shown that even in the upstream and stagnant region of the arc flow, turbulence enhances the heat transfer by a factor of 50–100 with reference to the molecular thermal conductivity. The radius of the arc column at current zero is in the order of 1 mm. Turbulence increases with the axial position in the downstream part of the nozzle.

The experiments reported in [24] concluded that turbulence eddies of different sizes lead to the distortion of the thin arc column shortly before current zero and the increase in arc voltage and resistance. Laminar flow prediction of the critical RRRV [25] is at least one order of magnitude lower than the measurement for both nitrogen and SF$_6$ [23]. The importance of turbulence in switching arcs was also confirmed by the work in [26], [27].

C. Contribution of Different Processes Towards Arc Cooling

In parallel to the commercial application of SF$_6$ in switching equipment, effort to theoretically understand the superior interruption capability of SF$_6$ in comparison with other gases, especially air, also started in the 1960 s. A typical example of the effort to relate the arc cooling time constant to the material properties can be seen in [28] where the relationship between temperature and electrical conductivity was used but the arc was treated as a uniform column of conducting gas with an a fixed overall cooling power. Around the same time, more sophisticated relationships for the time constant of current interruption in short line fault and the critical RRRV were both derived in [29]. While the important role of energy balance relating to arc cooling and the dependence of arc conductance on temperature were correctly identified, the difficulties in treating the distributed nature of arc cooling in strong gas flow rendered the approach very limited use in practice.

On the other hand, numerical solutions provide detailed results with excellent spatial and temporal resolution. The required assumptions are minimal. While the contribution of different energy exchange processes towards energy removal from the arc column were studied in [29], [30], [31], there is a lack of understanding on the contribution from each process towards the variation of the arc resistance or conductance.

In the present work, a method to quantify the arc cooling ability of different gases, with SF$_6$ and air as examples, is established. Its main novelty is the clear accountability of the role of different energy transport processes in influencing the change of arc resistance, which is a significant step forward from the work in [32] where the relative strength of each energy exchange process towards energy removal from the arc column is studied, but no link to the change of arc resistance was established.

D. Interruption Capability and Arc Cooling Ability

The term "arc cooling" appears frequently in literature, however its true meaning in relation to current interruption has not been mathematically defined. This term is re-visited in the present work (Section III-A) and a clearer definition is proposed. In addition, the term "interruption capability" is commonly reserved for the performance of a circuit breaker with a specific design. In this work, the term "arc cooling index" (ACI) is proposed to describe the ability of a gas for arc cooling and quenching under selected arcing conditions (geometry and gas pressure).

The arc model and the experimental cases are introduced in Section II with a discussion on the approximations made. The arc model is calibrated with one set of test result for SF$_6$ and air, and the selection of turbulence model parameter is justified. This is followed by the establishment of the arc cooling quantifying method in Section III. In Section IV, results are presented and analysed. Conclusions are drawn in Section V.

II. THE ARC MODEL AND THE EXPERIMENTAL CASES

A. The Arc Model

The governing equations of the arc flow are based on the time-averaged turbulent Naiver-Stokes equations in two-dimensional axisymmetric space with an additional partial differential equation for current continuity and the equation of state for the gas. These equations can be expressed in the following conservation form:

$$\frac{\partial \rho \phi}{\partial t} + \nabla \cdot \left(\rho \phi \vec{V} \right) - \nabla \cdot \left(\Gamma_\phi \nabla \phi \right) = S_\phi \tag{1}$$

where ϕ is the dependent variable to be solved, ρ the density, t the time and V the velocity vector of the gas. The source terms S_ϕ and diffusion coefficients Γ_ϕ are listed in Table I.

In Table I, the notations have their conventional meaning with the subscripts l and t denoting, respectively, the laminar and turbulent part of the diffusion coefficient. The expression for the viscous terms is given in [33] and will not be repeated. The material properties for the two gases are from [34], [35]. The approximate radiation model [36] based on the net emission coefficient (NEC) is adopted to calculate the radiative energy source of q in Table I. NEC is defined for an isothermal sphere of hot gas with a radius of R$_{NEC}$. When this concept is used for switching arcs, an equivalent R$_{NEC}$ needs to be defined at each axial position in the arc column [32], and this equivalent radius is called the emission radius in this work. It depends on

TABLE I
DETAILS OF THE TERMS AND COEFFICIENTS OF (1) IN CYLINDRICAL POLAR COORDINATE SYSTEM

Equation	ϕ	Γ	S_ϕ
Continuity	1	0	0
z-momentum	w	$\mu_l + \mu_t$	$-\partial P/\partial z + J_r B_\theta +$ viscous term
r-momentum	v	$\mu_l + \mu_t$	$-\partial P/\partial r - J_z B_\theta +$ viscous term
Enthalpy	h	$\nabla \cdot (k_l + k_t)\nabla T$	$\sigma E^2 - q + dP/dt +$ viscous dissipation
Current continuity	φ	σ	0

Fig. 1. Predicted critical RRRV for SF_6 and air at different upstream stagnation pressures with an imposed di/dt of -13.5 A/μs. Measurements are from [17].

the radial temperature profile at the axial position. The radiative energy emitted from the arc core (from axis to the position corresponding to 83% of the axis temperature) is calculated based on the NEC with an emission radius of $0.5(R_{83} + R_{3K})$, where R_{83} is the radius of the point corresponding to the 83% of the axis temperature and R_{3K} is the radius of 3000 K from the axis. 80% of the radiative flux from the arc core is absorbed in the region from R_{83} to R_{3K} (the net absorption zone) [37]. A reduction of the absorption percentage from 80% to 60% [38] for air only leads to 2% difference in the arc resistance. The NEC data are taken from [39] for SF_6 and [40] for air.

As stated in Section I, turbulence plays an important role in arc cooling near current zero. The simplest Prandtl mixing length model (PML) provides satisfactory prediction of the turbulent effect in switching arcs provided that the turbulence parameter is properly chosen [41], [42]. The PML can be expressed by:

$$\mu_t = \rho(cr_\delta)^2 \left(\left| \frac{\partial w}{\partial r} \right| + \left| \frac{\partial v}{\partial z} \right| \right) \quad (2)$$

where c is a turbulence parameter and r_δ [33] is the thermal radius of the arc defined as:

$$r_\delta = \sqrt{\frac{1}{\pi} \int_0^{R_{500}} \left(1 - \frac{T_{500}}{T} \right) 2\pi r dr} \quad (3)$$

where R_{500} is the radial distance of the 500 K isotherm from the axis. The use of 500 K as the boundary of the cold surrounding gas is based on the fact that cold gas in regions further beyond 500 K is hardly disturbed.

The focus of the present work is to understand and quantify the contributions of different energy exchange processes, the arc model needs to be verified first. The turbulence parameter is calibrated with the measurement in [17] at 1.53 MPa for SF_6 and 1.3 MPa for air. c is 0.042 for SF_6 and 0.076 for air. Results in Fig. 1 show that the predicted critical RRRVs without considering turbulence is far too low compared with the measurement [17], [43]. It is fair to state that the PML model adequately represents the turbulent effect for both gases over the large range of upstream pressure. Quantitative analysis of the results obtained with the PML model should correctly reflect the role of turbulence in arc cooling.
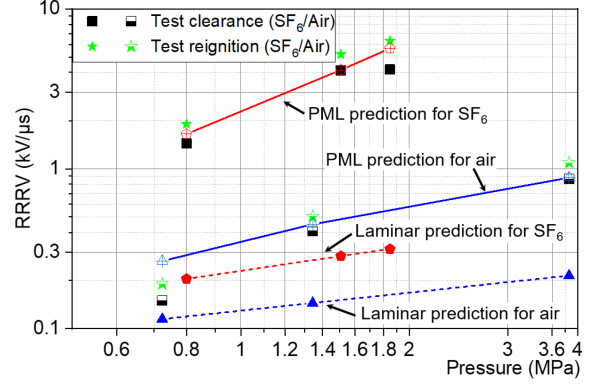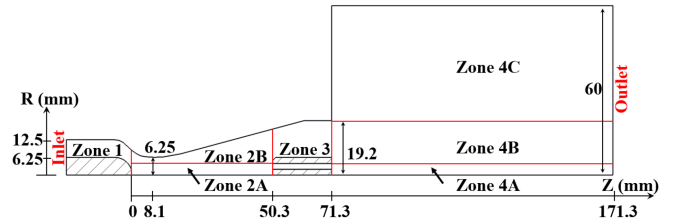

Fig. 2. Geometry of the computational domain based on information in [17].

B. Computational Domain, Initial and Boundary Conditions

The present work is based on the experimental cases reported in [17]. The computational domain shown in Fig. 2 includes a convergent–divergent nozzle, two electrodes and an exhaust tank (to maintain a constant background pressure).

The computation domain is divided into different zones, see Fig. 2. A total of 199 (axial) × 88 (radial) rectangular cells are used in Zone 2A. The size of the non-structured grids in other zones are also set appropriately so it does not affect the accuracy of solution in the arc region. The nozzle has a half expansion angle of 15°. Other dimensions are given in Fig. 2.

On the axis, axisymmetric conditions are imposed for all variables. Inlet and outlet boundary conditions are based on the test conditions in [17]. The mass, momentum, and enthalpy fluxes at the inlet are calculated by the isentropic relationships assuming an upstream stagnation temperature of 300 K and a stagnation pressure of P_0. The outlet pressure (P_e) is 0.25 of the inlet stagnation pressure. The nozzle wall is assumed to be thermally insulating and slippery to flow. No heat exchange between the gas and the electrodes are considered. Due to the very short arc duration ($< 74\,\mu$s), the effect of upstream electrode erosion is expected to be insignificant based on information provided in [44]. Version 19.1 of ANSYS Fluent was used to implement and solve the arc model.
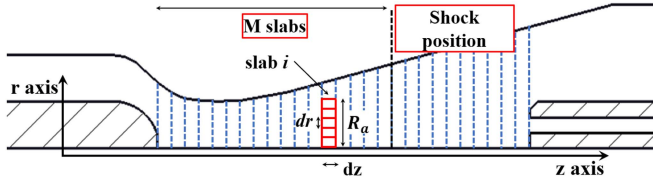
Fig. 3. Schematic diagram as basis for arc cooling analysis.

Fig. 4. Illustration of the main physical processes involved in arc cooling.

III. A NEW METHOD OF EVALUATING THE ARC COOLING ABILITY OF GASES

A. Derivation of Arc Cooling Effect

The rate of change of arc resistance before current zero is central to thermal interruption. The arc resistance is collectively determined by each section of the arc column. Arc cooling is a term that is often used in literature to refer to the effect of thermal energy removal from the conducting arc column. During the current zero period, arc cooling helps lower the arc temperature, reduce its size, and increase the arc resistance. Therefore, arc cooling over the current zero period ultimately refers to the effect in increasing the arc resistance, instead of only reducing the total energy content in the arc column. This effect can be quantitatively described by the rate of change of arc resistance (dR/dt), or the relative rate of change of arc resistance ($dR/dt/R$), giving a rate of percentage change in arc resistance.

As shown in Fig. 3, the arc column is segmented by structured grids (red grids as example). The arc resistance is the sum of the contributions from all segments between the two electrodes. At low current, the arc column is slender, and the radial electric field component is negligible. For each segment, or each slab as it is conveniently called, Ohm's law can be applied:

$$I = E_Z \int_{r=0}^{r=R_a} \sigma \cdot 2\pi r dr = E_Z \cdot G_i \qquad (4)$$

where G_i is the conductance of the ith slab scaled to a unit thickness $dz = 1$. R_a is the radius of the conducting column that is defined by a threshold electrical conductivity. dr and r are, respectively, the radial thickness of a grid cell and the radius of its centre.

Neglecting the relatively weak effect of pressure change on electrical conductivity, the change of electrical conductivity at a point in the arc is mainly affected by the change in specific enthalpy or gas temperature at constant pressure:

$$\frac{\partial \sigma (h, p)}{\partial t} \approx \frac{\partial \sigma}{\partial h} \frac{\partial h}{\partial t} = \left(\frac{1}{C_p} \frac{\partial \sigma}{\partial T} \right) \frac{\partial h}{\partial t} \qquad (5)$$

where C_p, h, T and σ are the specific heat capacity at constant pressure, specific enthalpy, temperature, and electrical conductivity, respectively. t is the time. With a slowly changing R_a, the rate of change of the arc conductance in the ith slab can be expressed as below, with the help of (5):

$$\frac{\partial G_i}{\partial t} = \int_{r=0}^{r=R_a} \frac{\partial \sigma}{\partial t} 2\pi r dr \approx \int_{r=0}^{r=R_a} \left(\frac{1}{C_p} \frac{\partial \sigma}{\partial T} \right) \frac{\partial h}{\partial t} 2\pi r dr \qquad (6)$$
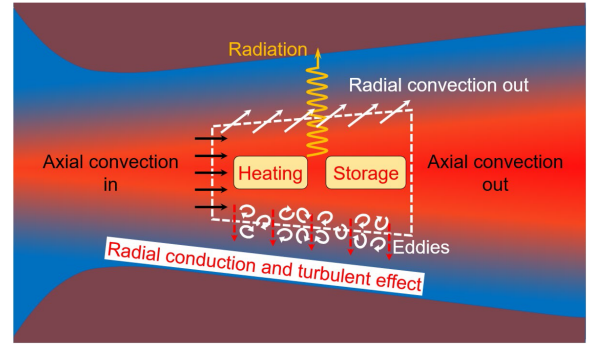
The term $\partial h/\partial t$ serves as a critical link between arc cooling (increase in arc resistance) and the energy content in the arc. It is to be noted that energy balance, as described by the governing energy equation, is based on energy density (ρh). A decrease of temperature in a grid cell does not mean its energy density will also decrease. This is because when the gas temperature decreases, the gas density increases, so the energy density may increase. It is therefore not accurate to use energy balance analysis to describe the effect of arc cooling. The governing energy equation can be rewritten as:

$$\frac{\partial h}{\partial t} = \frac{1}{\rho} \left(\sigma E^2 - q + \frac{dP}{dt} - \rho \vec{v} \nabla H \right.$$
$$\left. + \nabla \cdot (k_{eff} \nabla T) + G_D - \rho \frac{\partial}{\partial t} \left(\frac{V^2}{2} \right) \right) \qquad (7)$$

where H is the total specific enthalpy, $k_{eff} = k_l + K_t$, G_D the viscous and turbulence dissipation term and other variable have been given in Table I. Substituting (7) into (6) leads to an expression for the contributions of different processes towards the change of electrical conductance in a slab:

$$\frac{\partial G_i}{\partial t} = \int_{r=0}^{r=R_a} 2\pi r \frac{\partial \sigma}{\partial T} \frac{1}{\rho C_p} \left(\sigma E^2 - q + \frac{dP}{dt} \right.$$
$$\left. - \rho \vec{v} \nabla H + \nabla \cdot (k_{eff} \nabla T) + G_D - \rho \frac{\partial}{\partial t} \left(\frac{V^2}{2} \right) \right) \qquad (8)$$

B. Arc Cooling Effect Due to Different Processes

The main energy transport processes considered in (8) are illustrated in Fig. 4 where the arc is sustained by Ohmic heating. Radiation (yellow spring arrow) takes energy from the arc centre and part of it is absorbed at the arc edge. Axial convection (black arrows), radial convection (white arrows), and radial conduction (red dotted arrows) affect the cooling process. A positive effect is defined as one that tends to increase the arc resistance and help extinguish the arc. Conversely, a negative effect tends to decrease the arc resistance.

The right-hand side of (8) is split into 6 parts according to the processes shown in Fig. 4 which are:

1) *Ohmic and viscous heating (negative contribution)*

$$\left(\frac{\partial G_i}{\partial t}\right)_1 = \int_{r=0}^{r=R_a} 2\pi r \frac{\partial \sigma}{\partial T} \frac{1}{\rho C_p} \left(\sigma E^2 + G_D\right) dr$$

2) *Radiation (positive effect)*

$$\left(\frac{\partial G_i}{\partial t}\right)_2 = -\int_{r=0}^{r=R_a} 2\pi r \frac{\partial \sigma}{\partial T} \frac{q}{\rho C_p} dr$$

3) *Radial convection*

$$\left(\frac{\partial G_i}{\partial t}\right)_3 = \int_{r=0}^{r=R_a} 2\pi r \frac{\partial \sigma}{\partial T} \frac{1}{\rho C_p} \left(-\rho v \frac{\partial H}{\partial r}\right) dr$$

4) *Axial convection*

$$\left(\frac{\partial G_i}{\partial t}\right)_4 = \int_{r=0}^{r=R_a} 2\pi r \frac{\partial \sigma}{\partial T} \frac{1}{\rho C_p} \left(-\rho w \frac{\partial H}{\partial z}\right) dr$$

5) *Radial conduction (positive effect)*

$$\left(\frac{\partial G_i}{\partial t}\right)_5 = \int_{r=0}^{r=R_a} 2\pi r \frac{\partial \sigma}{\partial T} \frac{1}{\rho C_p} \left(\nabla \cdot (k_{eff} \nabla T)\right) dr$$

6) *Local pressure change*

$$\left(\frac{\partial G_i}{\partial t}\right)_6 =$$
$$\int_{r=0}^{r=R_a} 2\pi r \frac{\partial \sigma}{\partial T} \frac{1}{\rho C_p} \left(\frac{dP}{dt} - \rho \frac{\partial}{\partial t}\left(\frac{V^2}{2}\right)\right) dr$$

In the above expressions, the pressure work accounts for less than 1% towards the arc resistance change, which will not be included in the discussions below. Its fluence in energy balance calculation for low current arcs (< 2 kA) was also ignored in previous work [33], [45]. The relative rate of change of arc resistance for a single slab can then be derived as:

$$\frac{1}{R_i} \frac{dR_i}{dt} = -\frac{\sum_{k=1}^{5}\left(\frac{\partial G_i}{\partial t}\right)_k}{G_i} \tag{9}$$

where k represents the energy exchange processes. For the whole arc column, the total resistance is:

$$R_{arc} = \sum_{i=1}^{i=M} \frac{dz_i}{\int_0^{R_a} \sigma \cdot 2\pi r dr} = \sum_{i=1}^{i=M} \frac{dz_i}{G_i} \tag{10}$$

where M is the number of slabs or slices that the arc column is cut into by the structured grid system. The relative rate of change of arc resistance for the whole arc column is then:

$$\frac{1}{R_{arc}} \frac{dR_{arc}}{dt} = -\sum_{k=1}^{5} \frac{\sum_{k=1}^{5}\left(\sum_{i=1}^{M}\left(\frac{dz_i}{G_i^2}\left(\frac{dG_i}{dt}\right)_k\right)\right)}{\sum_{i=1}^{M} \frac{dz_i}{G_i}} \tag{11}$$

Representing the right-hand side of (11) by $1/\tau$, then the variation of R_{arc} with time will be:

$$R_2 = R_1 e^{\int_{t_1}^{t_2} \frac{dt}{\tau}} \tag{12}$$

where τ can be interpreted as a characteristic time of arc resistance growth and it may change with time. The quantity $1/\tau$ is thus a quantitative measure of the arc cooling effect in a flow field. The effect of arc cooling for each energy exchange
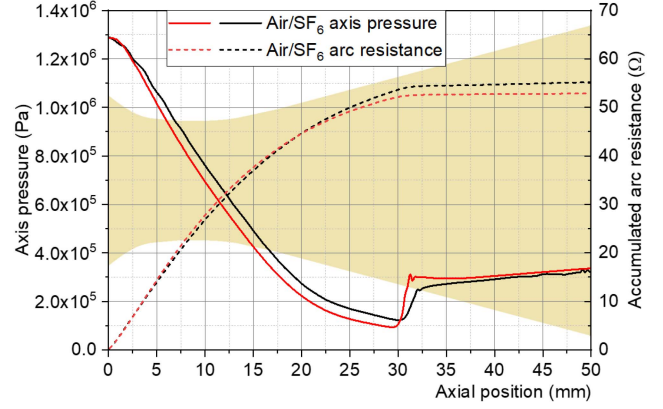

Fig. 5. Pressure on the axis and arc resistance build-up from the upstream electrode (0 mm) at 10 A before current zero. The yellow shade indicates the geometry of the nozzle for convenience of reference.

mechanism can be represented by its corresponding characteristic time, which can be written as $1/\tau_k$ as in (13). The smaller this characteristic time is, the stronger the arc is cooled.

$$\frac{1}{\tau} = \sum_{k=1}^{5} \frac{1}{\tau_k} = \sum_{k=1}^{5} -\frac{\sum_{i=1}^{M}\left(\frac{dz_i}{G_i^2}\left(\frac{dG_i}{dt}\right)_k\right)}{\sum_{i=1}^{M} \frac{dz_i}{G_i}} \tag{13}$$

IV. RESULTS AND DISCUSSIONS

The analysis of the relative importance of different energy exchange processes on arc cooling can be conveniently divided into two steps. In the first step (Section IV-B), analysis will focus on the variation of different energy exchange processes with respect to the axial position in the nozzle. This will provide a full picture of the distributed nature of arc cooling along the arc column. In the second step (Section IV-D), the overall arc cooling effect by each mechanism will be summarized and a quantitative indicator of the arc cooling effect for each gas is defined.

Conditions reported in [17] are used in this investigation. The current is linearly ramped down towards current zero at a constant di/dt of -13.5 A/μs. The method proposed in this work is applicable to other values of di/dt. Before the current is ramped down, a steady state arc at 1 kA is first obtained. The upstream stagnation pressure is 1.5 MPa, and the background pressure is 0.375 MPa.

Arc induced contact evaporation may occur at high current [46] or at low current with an arc duration of 1 ms or longer [47]. In the experiment [17], the upstream contact is set as the cathode, and it took only 74 μs for the current to decrease from 1 kA to zero. For such a short arc duration, no obvious contact erosion has been observed in [47]. Therefore, upstream electrode erosion is not considered in the present work.

A. Selection of Arc Length for Arc Cooling Analysis

Cooling by gas flow to the arc column is not uniform [48]. This is also true in the simulation results. Fig. 5 shows the position of the flow shock (axial position at 30 mm). Our results show

that the section of the arc column downstream the flow shock has weak contribution ($<5\%$) to the total arc resistance because of the broadening of the arc column, as reported in previous work [37], [48]. This is true for both SF_6 and air. Upstream the shock there is steep pressure gradient in the axial direction to accelerate the gas flow. For the study of the arc cooling ability of different gases due to the difference in their material properties, only the section of the arc column upstream the flow shock is considered. The maximum Mach number on the axis is 2.6 for SF_6 and 2.9 for air.

In previous work [49], the accuracy of the energy balance analysis is affected by the choice of the radial boundary of the conducting column where gas temperature is low, but density is high. With the method developed in Section III, this source of inaccuracy is eliminated as a result of the inclusion of the term $\partial\sigma/\partial T$ in the cooling terms $(\partial G_i/\partial t)_k$. Considering the difference in electrical conductivity between SF_6 and air the conducting column boundary is defined by the location of 5000 K for SF_6 and 4000 K for air.

It has to be noted that the arc cooling abilities of SF_6 and air are compared under identical arcing conditions including the nozzle geometry. The present work is not intended to compare the best possible cooling effect of the two gases, which is difficult to define. Giving the closeness in Mach number, the conclusions drawn in this should be representative.

B. Distributed Arc Cooling Along the Arc Length

When the arc current reduces its magnitude before current zero, the arc column size and the relative importance of the cooling mechanisms both changes. Four instantaneous currents (100 A, 50 A, 10 A and 0 A) were chosen to demonstrate the cooling dynamics. Details are given in Fig. 6. The curves were calculated from the simulation results according to (9).

Choosing air at 100 A as an example, the solid black curve is the overall result based on (9) and the positive values along the arc length mean that the electrical resistance for each slab of the arc column increases. The relative rate of change for arc resistance ($1/R_i*dR_i/dt$) is roughly 0.25/μs at the typical axial position of 20 mm. This implies that the arc resistance in the slab increases by 25% in one microsecond. The solid blue curve represents the cooling effect due to turbulence. At the axial position of 20 mm, it drives a cooling rate of 0.65/μs (65% increase in arc resistance in one microsecond), but Ohmic heating (solid red curve) cancels this cooling effect at almost the same rate.

The direction of convection matters in arc cooling. Over the axial locations from 15 mm to 30 mm, gas flows towards the nozzle wall in the radial direction for both air and SF_6 at 100 A. This outward flow tends to bring the hot gas out and broaden the arc column. An increased arc column leads to reduced arc resistance, therefore negative arc cooling rate. On the opposite, if cold gas flows inside the arc column, it tends to constrain the arc size and increase the arc resistance. In this case the arc cooling rate will be positive. This indeed happens in a small region near the upstream electrode at 100 A, and also in an extended region in the case at 0 A.

Radiation makes a very small contribution towards arc cooling. Therefore, the overall arc cooling effect at the axial position of 20 mm is only 0.25/μs at 100 A despite the velocity on axis reaches 4000 m/s. At 100 A, the arc cooling effects are close to each other for SF_6 (0.4–0.5/μs) and air (0.3/μs for air). In SF_6, radiation takes more energy away from the arc column. This is due to the higher axis temperature and a smaller arc radius. Radiation loss increases rapidly when the temperature increases in the range from 10 000 K to 20 000 K (proportional to the fourth power of temperature for ideal radiator). Ohmic heating is also stronger as a result of its small arc radius.

Moving towards lower current, arcs in SF_6 and air exhibit very different behaviour. The root cause is that SF_6 arc column shrinks faster than that in air. Firstly, the NEC is sensitive to the emission radius and increases rapidly when the emission radius reduces, implying that SF_6 arc emits more radiative energy at lower current. At 10 A, radiative cooling effect in SF_6 is much stronger than that in air (0.75/μs for SF_6 and 0.1/μs for air at 20 mm). Secondly, the axial electric field in SF_6 arc becomes higher than that in air when the current approaches zero. This leads to stronger Ohmic heating effect in the SF_6 arc, as clearly shown in Fig. 6. Thirdly, due to the reduced arc column size in SF_6 turbulent arc cooling (radial thermal conduction, solid blue curve) increases from 0.5/μs at 100 A to 5/μs at current zero, whereas in air turbulent arc cooling does not vary significantly. The overall effect at current zero is 7/μs for SF_6 and 0.6/μs for air, showing significant difference in their arc cooling ability in strong axial flow. It is evident that turbulence enhanced arc cooling is the main influencing factor, and its strength is closely related to the arc column size near current zero.

C. Arcs Dynamics

The fact that the arc cools down at different rates in SF_6 and air is also seen clearly in Fig. 7. At 500 A, the radius of the conducting column at the typical axial position of 20 mm, is 1.6 mm in SF_6 based on a conducting threshold temperature at 5000 K ($\sigma = 1$). In comparison, the conducting column's radius in air is 2.57 mm at a temperature of 4000 K ($\sigma = 1$). The ratio of the radius in SF_6 to that in air is 1:1.6. The highest temperature in SF_6 is 20 400 K while that in air is 17 900 K. Reaching current zero, the conducting radius is 0.23 mm in SF_6 and 1.3 mm in air. The ratio becomes 1:5.65. The difference in axis temperature and arc column size along the axial direction in the nozzle is given in Fig. 8.

Experiment in [50] show that the arc cooling time constant in strong gas flow is proportional to the arc cross sectional area. Besides turbulence, the present work also shows that radial convection can become important for thin arc column, as shown by the dotted red line in Fig. 6 for SF_6 arc at current zero when non-conducting cold gas enters the arc column (black arrows in lower half of Fig. 9 and dashed red curve for current zero of SF_6 in Fig. 6). For air, non-conducting gas enters the arc column up to the axial position of 15 mm contributing to arc cooling. but hot gas moves out of the arc column in the downstream region leading to heating effect. This is shown by the upper half in Fig. 9 and the diagram at current zero for air in Fig. 6.
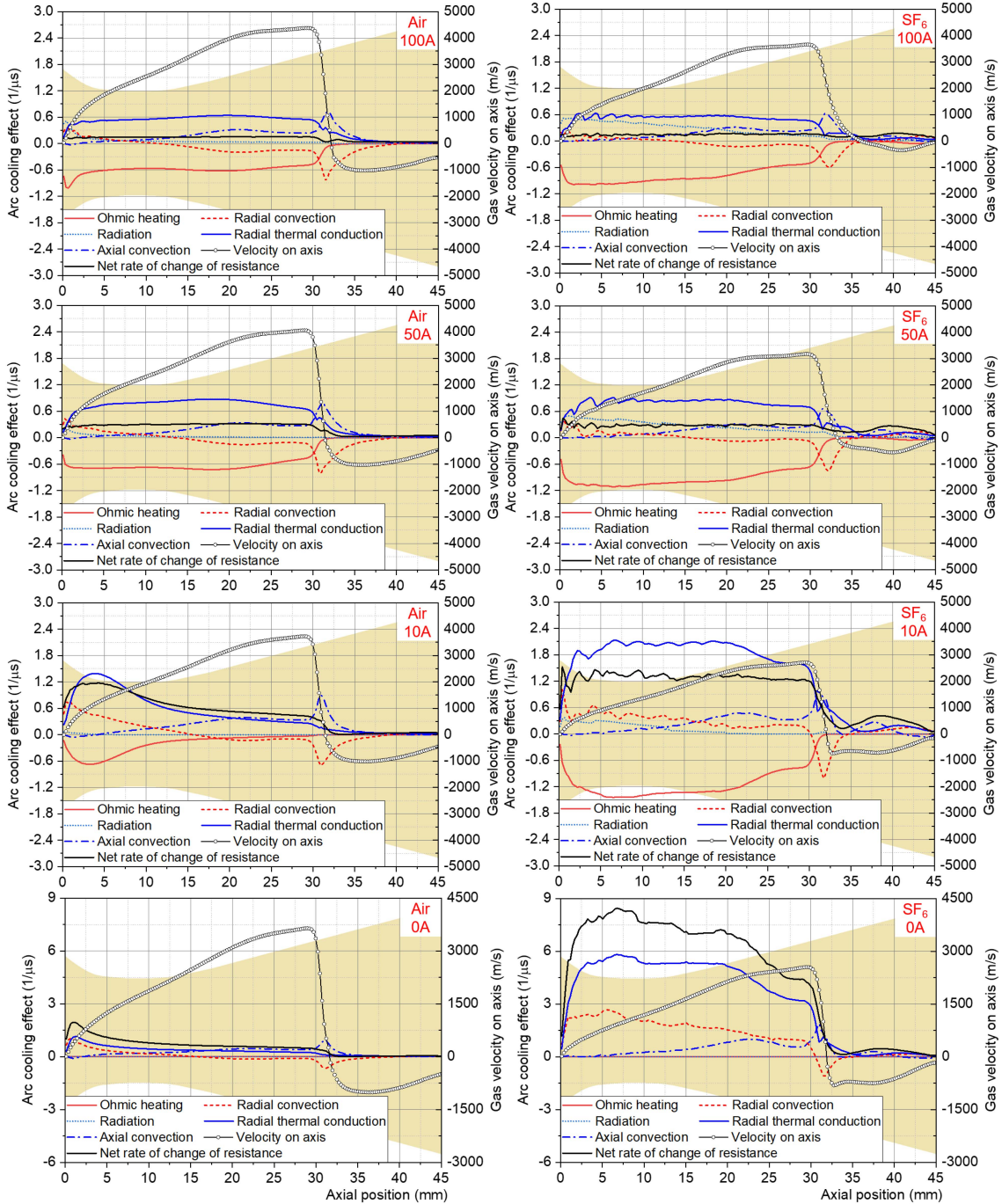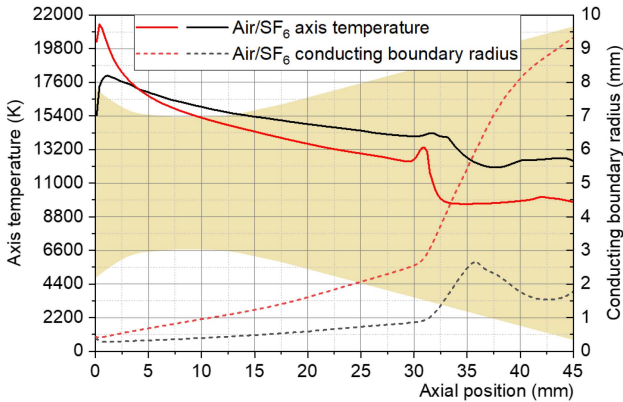
Fig. 6.   Variation in arc cooling effect of different mechanisms along the axis and their evolution towards current zero for nozzle arcs in air and SF_6.

The arc cooling behaviour of a gas is determined by its material properties. A qualitative explanation can be constructed by comparing the energy density, which is related to the product of specific heat capacity at constant pressure and mass density (ρCp), in the electrically conducting arc column and the surrounding gas [32], as well as the relative largeness of arc radius between the two gases as shown in Fig. 7, which again is related to ρCp through turbulent viscosity [32]. A thin arc column and low energy density inside the arc would benefit the thermal interruption process through faster arc cooling.

D. Variation of Arc Resistance Towards Current Zero and Quantitative Indicator for Arc Cooling Ability

The arc cooling effect of different mechanisms vary along the arc column as well as with time, as a result of the changes in flow field and current (di/dt). These changes collectively determine how the arc resistance evolve towards current zero and beyond. Adding up all the slabs based on (11) from the upstream electrode to the slab upstream the flow shock, the contribution by different mechanisms is presented in Fig. 10 over 8 instantaneous
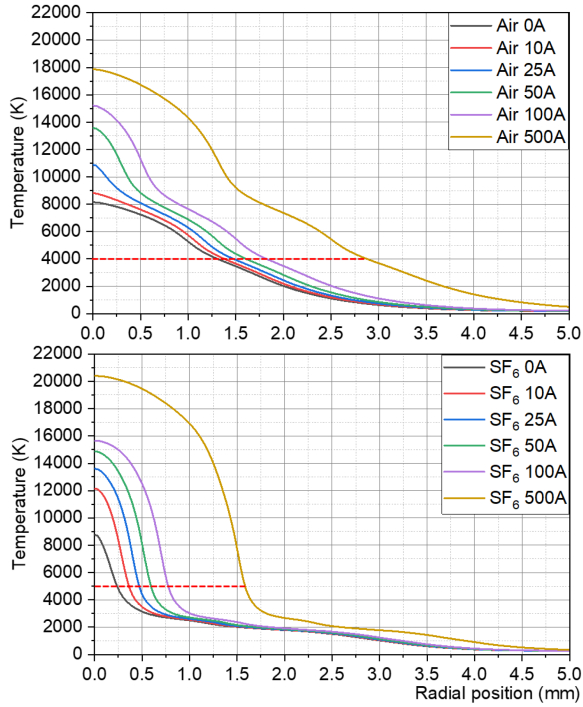
Fig. 7. Radial arc temperature profiles at z = 20 mm in air and SF_6.

Fig. 8. Axis temperature and arc column radius at 50 A for SF_6 and air.

Fig. 9. Variation of temperature (color contour) and radial velocity (arrows in grey scale) in air and SF_6 arcs at current zero. The 4000 K and 5,000 K isotherm gives an indication of the size of the conducting column.

Fig. 10. Relative importance of each energy exchange process (integrated over all slabs up to the flow shock) with respect to the total arc cooling effect. Blue represents turbulent cooling and negative values reduce the arc resistance.

current values from 1000 A to 0A. The bar chart is plotted in terms of the relative importance of each of the energy exchange process with respect to the total cooling effect, i.e., the sum of all positive terms evaluated in the right-hand side of (11). Therefore, the sum of all contributions for cooling is always 100%. It is to be emphasized here that the term "arc cooling effect" is defined as the ability of a process, such as turbulence or radial thermal conduction, to grow the arc resistance, measured as the relative increase of the arc resistance (the sign has to be positive).

From Fig. 10, Ohmic heating counter plays the cooling mechanisms, preventing the arc resistance from growing rapidly for current above 100 A. Radiation plays a decreasing role when the current approaches zero while turbulent arc cooling enhances. The following features are identified:

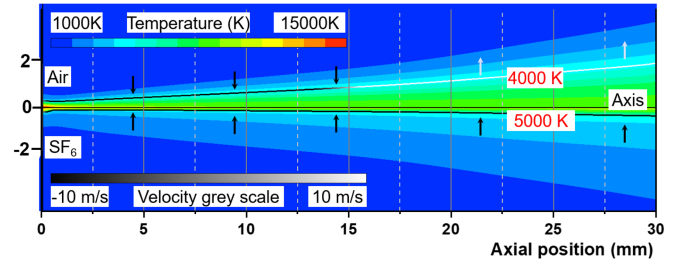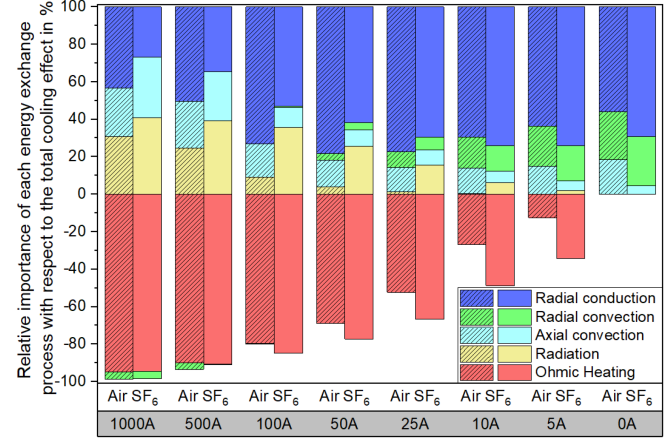- The relative strength of radial convective arc cooling increases towards current zero for both SF_6 and air (green

patches). For SF_6, there is an increase in the absolute power of arc cooling by radial convection (shown in Fig. 6). For air the absolute cooling power decreases (Fig. 6).

- Axial convective cooling is still significant in air arc at current zero. It takes about 20% of the arc cooling effect in air, while in SF_6 it is only 5%. This difference is related to the larger arc diameter as shown in Fig. 8.

Fig. 11 presents a summary of the arc cooling abilities of SF_6 and air. Focusing on the two green curves firstly, the variation in arc resistance can be calculated from (12) with a time dependent τ. The difference between arc resistance for SF_6 and air can be chased back with (13) with $1/\tau_k$ plotted in Fig. 11. The total $1/\tau$ is indicated by the solid black curves which are the summation of the effect of five energy exchange mechanisms.

A positive value leads to increase in arc resistance and a negative value reduces the arc resistance. Clearly the arc resistance in SF_6 increases much faster than that in air due to the accelerated increase of resistance in SF_6 caused by the smaller characteristic cooling time of radial conduction and radial convection. At current zero, the arc resistance in SF_6 (433 Ω) becomes roughly 4 time that in air (100 Ω).

E. Arc Cooling Index (ACI) of Gases

Returning to the question of assessing the arc cooling ability of a gas, which is mainly controlled by its material properties
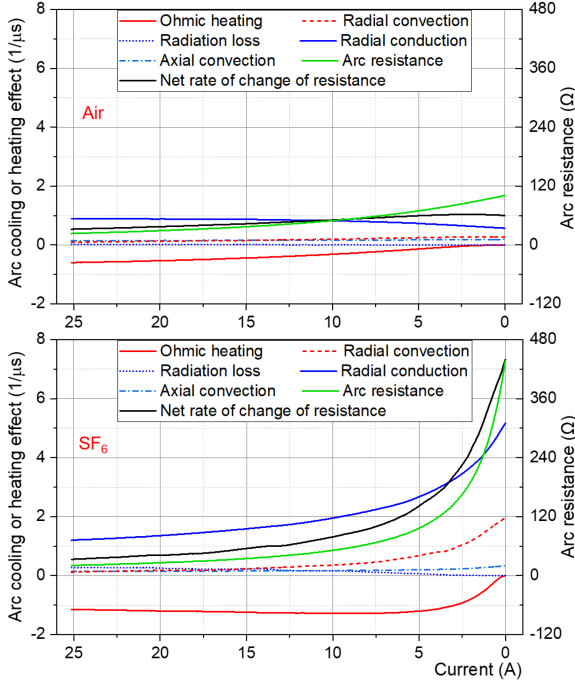
Fig. 11.   Variations of arc cooling or heating effect of different energy transport processes and evolution of arc resistance before current zero.
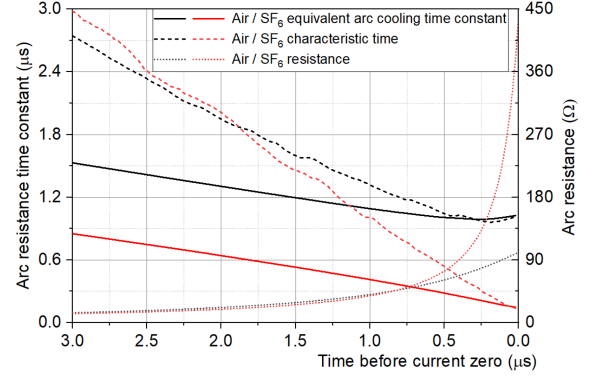

Fig. 12.   Arc cooling characteristic time (dotted lines) and the equivalent arc cooling time constant (solid lines) for SF_6 and air before current zero.

TABLE II
ARC COOLING INDEX OF SF_6 AND AIR BASED ON A CONVERGING-DIVERGING NOZZLE OF 15° HALF EXPANSION ANGLE, AN UPSTREAM PRESSURE OF 1.53 MPA AND A di/dt OF -13.5 A/μs.

Arc cooling index (ACI)	SF_6		Air	
	(1/μs)	(%)	(1/μs)	(%)
Overall ACI	2.59	100	0.96	100
Ohmic heating	-1.09	-42	-0.20	-20
Radiation	0.09	3	0.002	0
Radial convection	0.69	26	0.23	24
Axial convection	0.20	7	0.17	17
Turbulent mixing	2.70	104	0.76	79

The arc resistance increases at current zero is e^x where x is the ACI.

and weakly influenced by the design, it is necessary to define the conditions under which the ACI is evaluated. The present work is aimed at the establishment of the evaluation method and test it against known facts. The arcing geometry is a typical converging-diverging nozzle with a di/dt = -13.5 A/μs, equivalent to a 30 kArms power frequency current at 50 Hz.

The variation of the characteristic time (τ) describes the changing arc cooling environment when the arc current reduces. It is difficult to use such a changing quantity to characterizing the arc cooling ability of a gas. Replacing τ in (12) with a constant equivalent time constant between instant t before current zero and the current zero point, (11) can be rewritten as:

$$\tau_{eq} = \frac{-t}{\ln R_{cz} - \ln R_t} \quad (14)$$

where R_t and R_{CZ} are, respectively, the arc resistance at t (a negative value) before current zero and the arc resistance at current zero, calculated from (10). Plotting the instantaneous τ and the equivalent time constant τ_{eq} in Fig. 12, it can be seen that the two equivalent time constants are decreasing in parallel up to 1 μs before current zero. However, most of the difference in arc resistance is developed in the final 1 μs. It is thus a reasonable choice to use the reciprocal of the equivalent time constant at 1 μs as the arc cooling index (ACI) to differentiate the arc cooling abilities of the two gases. It is 2.59/μs for SF_6 and 0.96/μs for air. Further splitting into the different energy exchange mechanisms, it can be shown that (11) can be used to arrive at the following expression:

$$R_{CZ} = R_t \prod_{k=1}^{5} e^{\int_t^0 \frac{dt}{\tau_k}} = R_t \, e^{\sum_{k=1}^{5} \frac{1}{\tau_{eq,k}}} \quad (15)$$

and

$$\frac{10^{-6}}{\tau_{eq,\,k}} = \int_t^0 \frac{dt}{\tau_k} \quad (16)$$

where t = -10^{-6} s. The final results are given in Table II.

V. DISCUSSIONS AND CONCLUSION

A method has been developed in the present work for analysing and characterizing the arc cooling abilities of different gases with the aim to help search and select an alternative gas to SF_6 in high voltage switching applications. Using a single converging-diverging nozzle and one *di/dt* value before current zero, it is shown that the method is able to:
- quantitatively evaluate the contributions towards arc cooling from different energy exchange mechanisms, including Ohmic heating, radiation, radial convection, axial convection, and turbulent mixing, in space (different axial location in the nozzle) and in time.
- define an overall arc cooling index (ACI) for each gas. It is 2.59/μs for SF6 and 0.96/μs for air.
- split the overall ACI into contributions by different energy exchange mechanisms (see Table II) for profiling purposes.

The meaning of arc cooling is clarified. It is defined as the effect of an energy exchange process (Ohmic heating or turbulence as examples) on the increase of arc resistance. It is

not only about energy removal from the conducting arc column, as done in the previous work. This is because the total energy content in the conducting arc column may not always decrease when the arc is cooled down and electrical resistance increases.

The arc cooling effect of an energy exchange mechanism is defined as the reciprocal of a characteristic time ($1/\tau_k$) that changes in space and time due to changes in gas flow and current. Having identified the pattern of change of the overall equivalent arc cooling time constant (τ_{eq}), the ACI of a gas is proposed to be the reciprocal of the equivalent arc cooling time constant ($1/\tau_{eq}$) at 1μs before the current zero point since the arc resistance in SF_6 increases significantly in the very last microsecond before current zero. Depending on the arcing geometry, definition of ACI at a different time before current zero is also possible.

It is found that when applying the method to SF_6 and air, the arc cooling effects ($1/\tau_k$) of turbulence and radial convection keep increasing in SF_6 in the last 2 μs before current zero but they remain effectively unchanged in air. It is these two energy exchange mechanisms that make SF_6 superior to air for thermal interruption. At 500 ns before current zero, the overall equivalent arc cooling time constant in air is 4 times that in SF_6, and the diameter of the arc column in air is also 4 times that in SF_6. The air arc resistance at current zero is approximately ¼ that of SF_6.

It must be noted here that the accuracy of the method developed in the present work relies on the calibration of the turbulence model against the measured critical RRRV although one value is only needed. No measurement error was given in the relevant references despite the overall good agreement between the prediction and measured RRRV as reported in Section II. To quantify the ACI of other gases, the turbulence model has to be calibrated against at least one measured RRRV or arc resistance before current zero. In addition, when a different nozzle geometry is used, the ACI may change. For the purpose of benchmarking, a nozzle and typical arcing conditions have to be agreed before applying this method.

While it is expected that electrode erosion does not play an important role in the measured critical RRRV over the short arcing period of 74 μs, evidence from future experimental diagnosis would be helpful to confirm this assumption.

The last point to note is that the method from the present work is intended for quantifying the arc cooling ability of gases in simple nozzle arrangement. The results should not be directly compared with the thermal interruption results of different gases in circuit breakers where the dual flow design (including the use of a hollow contact), nozzle ablation or contact erosion at high current can severely modify the overall arc behaviour. The present work will nevertheless provide an essential tool for further work on benchmarking or ranking potential SF_6 alternative gases.

REFERENCES

[1] H. M. Ryan and G. R. Jones, *SF6 Switchgear*. London, U.K.: Peter Peregrinus, 1989, pp. 22–62.

[2] L. G. Christophorou, J. K. Olthoff, and D. S. Green, "Gases for electrical insulation and arc interruption: Possible present and future alternatives to pure SF_6," Nat. Inst. Sci, Techn., Washington, DC, USA, Tech. Rep. 1425, 1997.

[3] P. Glaubitz et al., "CIGRE position paper on the application of SF_6 in transmission and distribution networks," *Electra*, vol. 34, no. 274, pp. 34–39, 2014.

[4] C. Preve, G. Lahaye, M. Richaud, R. Maladen, T. Penelon, and S. Galas, "Hazard study of medium-voltage switchgear with SF_6 alternative gas in electrical room," *CIRED-Open Access Proc. J.*, vol. 1, pp. 198–201, 2017.

[5] D. Dufournet, "Circuit breakers go high voltage," *IEEE Power Energy Mag.*, vol. 7, no. 1, pp. 34–40, Jan./Feb. 2009.

[6] H. B. Singh, L. Salas, H. Shigeishi, and A. Crawford, "Urban-nonurban relationships of halocarbons, SF_6, N_2O, and other atmospheric trace constituents," *Atmospheric Environ.*, vol. 11, pp. 819–828, 1977.

[7] R. Leifer, *Project AIRSTREAM: Trace gas Final Report, EML-549*. New York, NY, USA: U.S. Dept. Energy, Dec. 1992.

[8] M. Rigby, J. Muhle, and B. R. Miller, "History of atmospheric SF_6 from 1973 to 2008," *Atmos. Chem. Phys.*, vol. 10, no. 21, pp. 10305–10320, 2010.

[9] K. Protocol, *Kyoto Protocol. UNFCCC Website*, 1997. [Online]. Available: http://unfccc.int/kyoto_protocol/items/2830.php

[10] European Commission, *Green Deal: Phasing Down Fluorinated Greenhouse Gases and Ozone Depleting Substances*, 2022. [Online]. Available: https://ec.europa.eu/commission/presscorner/detail/en/IP_22_2189

[11] Y. Kieffel, T. Irwin, P. Ponchon, and J. Owens, "Green gas to replace SF_6 in electrical grids," *IEEE Power Energy Mag.*, vol. 14, no. 2, pp. 32–39, Mar./Apr. 2016.

[12] Y. Kieffel and F. Biquez, "SF_6 alternative development for high voltage Switchgears," in *Proc. IEEE Elect. Insul. Conf.*, 2015, pp. 379–383.

[13] B. Zhang, L. Chen, X. Li, Z. Guo, Y. Pu, and N. Tang, "Evaluating the dielectric strength of promising SF_6 alternatives by DFT calculations and DC breakdown tests," *IEEE Trans. Dielectrics Elect. Insul.*, vol. 27, no. 4, pp. 1187–1194, Aug. 2020.

[14] W. Y. Lee, J. U. Jun, H. S. Oh, J. K. Park, Y. H. Oh, and K. D. Song, "Comparison of the interrupting capability of gas circuit breaker according to SF_6, g^3 and CO_2 /O_2 mixture," *Energies*, vol. 13, 2020, Art. no. 23.

[15] J. Mantilia, "Switching interruption performance comparison between SF_6, CO_2 and fluoroketones-based mixtures in HVCB," CIGRE, Paris, France, Tech. Rep. A3-019, 2017.

[16] G. Frind, R. E. Kinsinger, R. D. Miller, H. T. Nagamatsu, and H. O. Noeske, "Fundamental investigation of arc interruption in gas flows," General Electric Co., Schenectady, NY, USA, Tech. Rep. EPRI EL-284, 1977.

[17] G. Frind and J. A. Rich, "Recovery speed of axial flow gas blast interrupter: Dependence on pressure and di/dt for air and SF_6," *IEEE Trans. Power App. Syst.*, vol. PAS-93, no. 5, pp. 1675–1684, Sep. 1974.

[18] D. Leseberg and G. Pietsch, "Optical investigations on a SF_6 switching arc inside a glass nozzle," in *Proc. 7th Int. Conf. Gas Discharges Appl.*, 1982, pp. 9–12.

[19] D. R. Airey, R. E. Kinsinger, P. H. Richards, and J. D. Swift, "Electrode vapor effects in high current gas blast switchgear arcs," *IEEE Trans. Power App. Syst.*, vol. PAS-95, no. 1, pp. 1–13, Jan. 1976.

[20] H. J. Schoetzau, H. P. Meili, E. Fischer, C. Strurzenegger, and H. P. Graf, "Dielectric phase in an SF_6 breaker," *IEEE Trans. Power App. Syst.*, vol. PAS-104, no. 7, pp. 1897–1902, Jul. 1985.

[21] E. Schade and K. Ragaller, "Dielectric recovery of an axially blown SF_6-arc after current zero: Part I-Experimental investigations," *IEEE Trans. Plasma Sci.*, vol. 10, no. 3, pp. 141–153, Sep. 1982.

[22] W. Hermann, U. Kogelschatz, L. Niemeyer, K. Ragaller, and E. Schade, "Experimental and theoretical study of a stationary high-current arc in a supersonic nozzle flow," *J. Phys. D: Appl. Phys.*, vol. 7, no. 12, pp. 1703–1722, Aug. 1974.

[23] W. Hermann and K. Ragaller, "Theoretical description of the current interruption in high voltage gas blast circuit breakers," *IEEE Trans. Power App. Syst.*, vol. 96, no. 5, pp. 1546–1555, Sep. 1977.

[24] W. Hermann, U. Kogelschatz, L. Niemeyer, K. Ragaller, and E. Schadl, "Investigation on the physical phenomena around current zero in HV gas blast breakers," *IEEE Trans. Power App. Syst.*, vol. PAS-95, no. 4, pp. 1165–1176, Jul. 1976.

[25] J. J. Lowke and H. Lee, "A numerical study of a two-dimensional circuit-breaker arc during current interruption," in *Proc. 8th Int. Conf. Gas Discharges Their Appl.*, 1985, pp. 54–56.

[26] M. T. C. Fang, Q. Zhuang, and X. J. Guo, "Current-zero behaviour of an SF_6 gas-blast arc. II. Turbulent flow," *J. Phys. D: Appl. Phys.*, vol. 27, no. 1, pp. 74–83, Jan. 1994.

[27] A. Kadivar and K. Niayesh, "Effects of fast elongation on switching arcs characteristics in fast air switches," *Energies*, vol. 13, no. 18, 2020, Art. no. 4846.

[28] W. Hertz, H. Motschmann, and H. Wittel, "Investigations of the properties of SF_6 as an arc quenching medium," *Proc. IEEE*, vol. 59, no. 4, pp. 485–492, Apr. 1971.

[29] B. W. Swanson and R. M. Roidt, "Boundary layer analysis of an SF_6 circuit breaker arc," *IEEE Trans. Power App. Syst.*, vol. PAS-90, no. 3, pp. 1086–1093, May 1971.

[30] D. T. Tuma, "A Comparison of the behaviour of SF_6 and N_2 blast arcs around current zero," *IEEE Trans. Power App. Syst.*, vol. PAS-99, no. 6, pp. 2129–2137, Nov. 1980.

[31] W. Hermann, U. Kogelschatz, K. Ragaller, and E. Schade, "Investigation of a cylindrical axially blown high-pressure arc," *J. Phys. D: Appl. Phys.*, vol. 7, no. 4, pp. 607–649, 1974.

[32] Y. Guo, H. Zhang, Y. Yao, Q. Zhang, and J. D. Yan, "Mechanisms responsible for arc cooling in different gases in turbulent nozzle flow," *Plasma Phys. Technol. J.*, vol. 4, no. 3, pp. 234–240, 2017.

[33] Q. Zhang, J. D. Yan, and M. T. C. Fang, " The modelling of an SF_6 arc in a supersonic nozzle: I. cold flow features and dc arc characteristics," *J. Phys. D: Appl. Phys.*, vol. 47, no. 21, 2014, Art. no. 215201.

[34] L. S. Frost and R. W. Liebermann, "Composition and transport properties of SF_6 and their use in a simplified enthalpy flow arc model," *Proc. IEEE*, vol. 59, no. 4, pp. 474–485, Apr. 1971.

[35] J. M. Yos, "Transport properties of nitrogen hydrogen oxygen and air to 30000 K," Tech. Rep. 1963-03-22, 1963.

[36] J. F. Zhang, M. T. C. Fang, and D. B. Newland, "Theoretical investigation of a 2-kA arc in a supersonic nozzle," *J. Phys. D: Appl. Phys.*, vol. 20, pp. 368–379, 1987.

[37] J. D. Yan, M. T. C. Fang, and C. Jones, "Electrical and aerodynamic behaviour of arc under shock conditions," *IEEE Trans. Plasma Sci.*, vol. 25, no. 5, pp. 840–845, Oct. 1997.

[38] V. R. Malghan, M. T. C. Fang, and G. R. Jones, "Investigation of quasi-steady state high current arcs in an orifice air flow," *J. Appl. Phys.*, vol. 48, pp. 2331–2337, 1977.

[39] R. W. Liebermann and J. J. Lowke, "Radiation emission coefficient for SF_6 arc plasma," *J. Quantitative Spectrosc. Radiative Transfer*, vol. 16, pp. 253–264, 1976.

[40] P. J. Shayler and M. T. C. Fang, "Radiation transport in wall-stabilized nitrogen arcs," *J. Phys. D: Appl. Phys.*, vol. 11, no. 12, pp. 1743–1756, Aug. 1978.

[41] J. D. Yan, K. I. Nuttall, and M. T. C. Fang, "A comparative study of turbulence models for SF_6 arcs in a supersonic nozzle," *J. Phys. D: Appl. Phys.*, vol. 32, pp. 1401–1406, 1999.

[42] Q. Zhang, J. Liu, J. D. Yan, and M. T. C. Fang, "The modelling of an SF_6 arc in a supersonic nozzle: II. Current zero behaviour of the nozzle arc," *J. Phys. D: Appl. Phys.*, vol. 49, no. 33, 2016, Art. no. 335501.

[43] A. Kadivar and K. Niayesh, "Dielectric recovery of ultrafast-commuting switches used for HVDC and fault current limiting applications," in *Proc. 5th Int. Conf. Electric Power Equip. Switching Techn.*, 2019, pp. 295–299.

[44] D. C. Strachan, "Radiation losses from high-current free-burning arcs between copper electrodes," *J. Phys. D: Appl. Phys.*, vol. 6, no. 14, pp. 1712–1723, 1973.

[45] J. Liu, Q. Zhang, J. D. Yan, J. Zhong, and M. T. C. Fang, "Analysis of the characteristics of DC nozzle arcs in air and guidance for the search of SF 6 replacement gas," *J. Phys. D: Appl. Phys.*, vol. 49, no. 43, 2016, Art. no. 435201.

[46] G. H. Gessinger and K. N. Melton, "Burn off behaviour of W-Cu contact materials in an electric arc," *Powder Metall. Int.*, vol. 9, no. 2, pp. 67–72, 1977.

[47] A. Kadivar and K. Niayesh, "Two-way interaction between switching arc and solid surfaces: Distribution of ablated contact and nozzle materials," *J. Phys. D: Appl. Phys.*, vol. 52, no. 40, 2019, Art. no. 404003.

[48] M. T. C. Fang, S. Kwan, and W. Hall, "Arc-shock interaction inside a supersonic nozzle," *IEEE Trans. Plasma Sci.*, vol. 24, no. 1, pp. 85–86, Feb. 1996.

[49] J. Liu, "Modelling and simulation of air and SF_6 switching arcs in high voltage circuit breakers," Ph.D. dissertation, Dept. Electrical Eng. The Univ. Liverpool, Liverpool, U.K., 2016.

[50] K. Ragaller, W. Egli, and K. P. Brand, "Dielectric recovery of an axially blown SF_6-Arc after current zero: Part II-theoretical investigations," *IEEE Trans. Plasma Sci.*, vol. 10, no. 3, pp. 154–162, Sep. 1982.

Kaiyuan Zhang received the B.Sc. and M.Sc. degrees from North China Electric Power University, Beijing, China, in 2014 and 2018, respectively, and the Ph.D. degree in electrical engineering from the University of Liverpool, Liverpool, U.K., in 2023. He is currently a Research Associate with the Department of Electrical Engineering and Electronics, University of Liverpool. His research interests include modeling of switching arcs and theory of SF_6 alternative gases.

Sili Yao received the B.Eng. degree in engineering physics from Tsinghua University, Beijing, China, in 1987. He is currently a Senior Engineer with professorial grade and Chief Expert of Xi'an High Voltage Apparatus Research Institute, Xi'an, China. He has long been engaged in the study and development of certifying test technologies for extra- and ultra- high voltage AC and DC electrical apparatuses. He is also the Chairman of China High Power Testing Liaison Technical Committee and Vice Chairman of CIGRE China National Committee SC A3.

Yi Wu (Senior Member, IEEE) received the B.Eng. degree from Xi'an Jiaotong University, Xi'an, China, in 1998, the M.Eng. degree from the Shenyang University of Technology, Shenyang, China, in 2002, and the Ph.D. degree from Xi'an Jiaotong University in 2006.

He is currently a Professor with XJTU and Holder of the National Science Fund for Distinguished Young Scholars. His main research interests include DC switching technology and switching arc simulation and diagnosis. He also sits on the Scientific Committee of the International Conference on gas discharges and their applications.

Jiu Dun Yan (Senior Member, IEEE) received the B.Eng. and M.Eng. degrees in engineering mechanics from Tsinghua University, Beijing, China, in 1986 and 1988, respectively, and the Ph.D. degree in electrical engineering from the University of Liverpool, Liverpool, U.K., in 1998.

He is currently a Professor of applied electromagnetism with the University of Liverpool. His research interests include theory of SF_6 alternative gases for switching applications, simulation and experiment of switching arcs, novel switching and insulation technology, and energy storage systems. Prof. Yan sits on the scientific committee of two international conferences (Physics of Switching Arcs and Gas Discharges and Their Applications). He is also a Member of the Current Zero Club.